RSC Advances

ROYAL SOCIETY OF CHEMISTRY

www.rsc.org/advances

1   **Competitive removal of Cd (II) and Pb (II) by biochars produced from**

2   **water hyacinths: performance and mechanism**

3

4   Yang Ding[a,b], Yunguo Liu[a,b, *], Shaobo Liu[c,d, *], Zhongwu Li[a,b], Xiaofei Tan[a,b], Xixian

5   Huang[a,b], Guangming Zeng[a,b], Yaoyu Zhou[a,b], Bohong Zheng[c], Xiaoxi Cai[a,b]

6

7   [a]College of Environmental Science and Engineering, Hunan University, Changsha

8   410082, PR China.

9   [b]Key Laboratory of Environmental Biology and Pollution Control (Hunan University),

10   Ministry of Education, Changsha 410082, PR China.

11   [c]School of Architecture and Art Central South University, Central South University,

12   Changsha 410082, P. R. China.

13   [d]School of Metallurgy and Environmental, Central South University, Changsha 410083,

14   P.R. China

15
16
17
18

[*] Corresponding author: Tel.: +86 731 88649208; Fax.: +86 731 88822829

E−mail: hnliuyunguo@163.com (Y.G. Liu).

[*] Corresponding author: Tel.: +86 731 88830923; Fax.: +86 731 88710171

E−mail: liushaobo23@aliyun.com (S.B. Liu).

19   **Abstract**

20   Three biochars converted from water hyacinths biomass at 300, 450, and 600 ^{o}C

21   were used to investigate the adsorption properties of Cd^{2+} and Pb^{2+}. In addition, the

22   competitive adsorption mechanisms between Cd^{2+} and Pb^{2+} were also conducted.

23   Adsorption kinetics and isotherms indicated that the maximum adsorption capacity of

24   Pb^{2+} was larger than that of Cd^{2+}, and the adsorption process in the mixed solutions of

25   two heavy metals (Cd^{2+} and Pb^{2+}) was more favorable for Pb^{2+}. Further investigation

26   about characterization of biochars demonstrated that cation exchange, surface

27   complexation, cation-π interaction and precipitation were the main mechanisms

28   responsible for the heavy metals removal. In this study, competitive adsorption may also

29   be explained by these mechanisms. These results are useful for the application of

30   biochars in selective adsorption and in practical wastewater treatment.

31

32

33

34

36

37

38   **1. Introduction**

39   Heavy metals may cause serious problems of environmental pollution and threaten

40   public health due to their toxic and non-biodegradable nature.[1] They are mainly

41   discharged from human activities such as metal plating, mining and paper industries.

42   Cadmium, lead, chromium, and nickel are the most common heavy metal pollutants

43   which could pose a risk to human health even under micro-concentration.[2,3] Therefore,

44   some cost-effective methods are needed to be developed to remove heavy metal

45   compounds from waste water. Most of traditional water treatment technologies have

46   disadvantages of either low efficiency or overspend. Biosorbents have attracted wide

47   concern in recent years because of the universality of materials and the high efficiency

48   of adsorption.

49   Although activated carbon (AC) has been used to remove various pollutants,[4,5] the

50   costs of the AC application in the treatment is higher than that of biochar. Moreover,

51   biochar is characterized by high affinity for contaminants in literatures,[6,7] thus it

52   potentially may be an alternative for AC. Biochar is a form of carbon black produced

53   through the thermal pyrolysis process of biomass under inert atmosphere conditions.

54   There are many types of biomass such as wood waste, crop residues, organic wastes,

55   which have been utilized as feedstock for biochar production.[8-10] Biochar has been

56   widely applied for removing toxic substances from waste water. For instance, Dong, et

57   al. found that biochar produced from sugar beet tailing had a strong affinity for Cr (VI)

58   with the sorption capacity of 123 mg g^{-1}.[11] Similarly, Gan, et al. indicated that biochar

59   produced from sugarcane bagasse had a good adsorption capacity for Cr (VI).[12]

60   Compared to biochar derived from hardwood, corn straw biochar had a good adsorption

61   capacity for both Zn (II) and Cu (II).[13] In addition, Kim, et al. demonstrated that the Cd

62   removal capacity of biochar produced from a giant Miscanthus increased with the

63   increasing of pyrolytic temperatures.[14]

64   However, pollution of multiple heavy metals is commonly existed in practical

65   wastewater. Therefore, it is inevitable to study the adsorption properties and

66   mechanisms of biochar in a mixed solution of several heavy metals. Chen, et al.

67   reported that Cu (II) would compete with Zn (II) for binding sites at Cu (II) and Zn (II)

68   concentrations $\geq$ 1.0 mM.[13] In our previous study, Pb (II) adsorption at high

69   concentrations would be inhibited by the competition from phenol in binary system, but

70   phenol adsorption was scarcely affected due to the directly phenol molecular adsorption

71   pattern.[15] Little competition occurred between Pb and atrazine for sorption on

72   dairy-manure derived biochar, while strong competition was observed on a commercial

73   activated carbon.[16] As two kinds of common heavy metals pollutants, further studies

74   focused on the mechanisms of competitive adsorption between Cd (II) and Pb (II) are

75   also needed to be conducted.

76   In Xiangjiang river basin, seasonal outbreak of water hyacinth is favored by the

77   subtropical monsoon climate. Water hyacinth has been considered as aggressive

78   invasive species by IUCN (the international Union for Conservation of nature). The

79   aggressive invasion of water hyacinth could pose threats to native ecosystem, including

80   depleting the water of oxygen and destroying the native biodiversity. The conversation

81   of water hyacinth into biochar and then application in the treatment of pollutants may be

82   environment friendly.

83   In this study, water hyacinths were used to prepare biochars via slow pyrolysis at

84   different pyrolysis temperatures ranged from 300 to 600 $^{\circ}$C. The resulted biochars were

85   applied to adsorb contaminants from aqueous solutions contained Cd (II), Pb (II), and

86   the mixture of Cd (II) and Pb (II). The specific objectives of this study were to (i)

87   examine Cd and Pb sorption isotherms and kinetics onto biochars; (ii) investigate the

88   underlying mechanisms governing Cd^{2+} and Pb^{2+} adsorption by biochars; (iii) explore

89   the properties of competitive adsorption between Cd^{2+} and Pb^{2+}; (iv) understand the

90   influence of three biochars on Cd^{2+} and Pb^{2+} adsorption and determine the optimal

91   pyrolysis temperature.

92   **2. Materials and methods**

93   **2.1 Biochar preparation**

94   Water hyacinths (WHs) were collected in Changsha, Hunan province, China. WHs

95   were washed with ultrapure water three times to remove the attached dust, and then

96   dried at 90 $^{\circ}$C for more than 24 h. The biochar samples (BCs) used in this study were

97   produced by slowly pyrolyzing the dried WHs in a lab-scale pyrolyzer (SK-G08123K,

98   China) under N_2 at 300, 450, and 600 $^{\circ}$C for 2 h. The reactor was heated with a heating

99   rate of 5 $^{\circ}$C min^{-1}. These biochars were cooled to room temperature under a nitrogen

100   condition. BCs were ground through a 0.15 mm sieve for this experiment. The biochars

101   obtained at different temperatures are referred to as BC300, BC450, and BC600,

102   respectively. Finally, they were stored in desiccators before use.

103   **2.2 Biochar characterization**

104   The elements of BCs were analyzed by an ESCALAB 250Xi X-ray Photoelectron

105   Spectrometer (XPS) (Thermo Fisher, USA). Brunauer, Emmett and Teller (BET) surface

106   area was determined using a gas sorption analyzer (Quantachrome Quadrasorb SI, USA)

107   and the total pore volume was examined from the N_2 adsorption-desorption isotherms.

108   Functional groups of biochar's surface were measured by a Fourier transform infra-red

109   spectrophotometer (FTIR) (Nicolet Magna-IR 750, USA). A scanning electron

110   microscopy (SEM) (JSM-7001F, Japan) was used to analyze the surface features of BCs

111   before and after adsorption. The pH of the point of zero charge (pH_{pzc}) was measured

112   using Electroacoustic Spectrometer (ZEN3600 Zetasizer, UK) by adding 0.1 g BCs to

113   solution with pH range from 1.0 to 10.0. Inductively coupled plasma-atomic emission

114   spectrometry (ICP-AES) (Baird PS-6, USA) was selected to detect the concentrations of

115   released cations from BC450.

116   **2.3 Batch adsorption and desorption experiments**

117   Ultrapure water with a resistivity of 18.25 MΩ cm^{-1} was used in this study. Cd^{2+}

118   and Pb^{2+} stock solution (1000 mg L^{-1}) were prepared by dissolving analytical grade

119   2.7442 g cadmium nitrate tetrahydrate ($Cd(NO_3)_2 \cdot 4H_2O$) and analytical reagent 1.5985

120   g lead nitrate ($Pb(NO_3)_2$) into 1000 mL ultrapure water, respectively. In single system,

121   these stock solutions were diluted to 50-900 mg L^{-1}. In binary system, the

122   concentrations of Cd^{2+} and Pb^{2+} (0.25−2 mmol L^{-1}) were prepared.

123   The impact of pH on biochar adsorption was examined by adjusting the initial Cd^{2+}

124   solutions (100 mg L^{-1}) ranging from 2.0 to 7.0, as well as Pb^{2+} solutions (100 mg L^{-1})

125   ranging from 2.0 to 5.0, considering the formation of precipitates under high solution

126   pH (Cd >7; Pb >5). The initial pH of different Cd^{2+}, Pb^{2+}, and the mixture solutions

127   were both adjusted to 5 by adding 1 M NaOH or 1 M HCl. Sorption kinetic was

128   conducted by adding 0.1 g biochar (BC300, BC450, and BC600) to 50 mL of the 100

129   mg L^{-1} solutions. These suspensions were shaken at 140 rpm at 30 $^{\circ}C$ for the designated

130   time periods. Experiments for adsorption isotherms were conducted at the initial

131   concentrations of solutions (50, 100, 150, 200, 250, 400, 500, and 900 mg L^{-1}) and the

132   shaking period of 24 h. In order to studying the competitive adsorption mechanisms

133   between Cd^{2+} and Pb^{2+}, 0.25 or 0.5 mmol L^{-1} Pb^{2+} (Cd^{2+}) was added into the prepared

134   Cd^{2+} (Pb^{2+}) solutions. Thermodynamic data were obtained at the temperature of 25, 30,

135   and 40 $^{\circ}C$ based on the experiments of adsorption isotherms. The influence of

136   background ionic strength on adsorption was studied at appropriate pH with the addition

137   of different concentrations of NaCl (0, 0.005, 0.01, 0.05, 0.1, 0.2, 0.5, and 1.0 mol L^{-1}).

138   BC450 with 0.1 g was added into each solution, and suspensions were shaken at 140

139   rpm under 30 $^{\circ}C$ for 24 h. The amount of cations (K, Ca, Na and Mg) released from

140   BC450 after Cd or Pb sorption was determined. Aliquots of biochar were added to Cd or

141   Pb solution (500 mg L^{-1}) and ultrapure water (control), respectively, at a 1:20 ratio

142   followed by agitation for 24 h. The concentrations of K, Ca, Na and Mg in the filtrate

143 were determined using ICP-AES. The net cations released were calculated by

144 subtracting cations released in control.

145 Desorption experiment included the following steps: 0.1 g biochar (BC300, BC450,

146 BC600) was added into 50 mL of 500 mg L^{-1} heavy metal solution and shaken at 140

147 rpm and 30 $^{\circ}$C for 24 h. Then the suspensions were filtered (0.22 μm filter) and biochars

148 were rinsed three times with ultrapure water. Biochars which have been used to sorb

149 heavy metals were then added into the solution of HCl (0.5 mol L^{-1}) and shaken for 24

150 h.

151 **2.4. Heavy metal analysis**

152 All experiments suspensions were filtrated, and then the residual concentration of

153 each heavy metal in the filtrate (0.22 μm filter) were determined using atomic

154 absorption spectrometer (AAS) (AAnalyst700, Perkin-Elmer, US). The adsorption

155 capacity ($Q_{e)}$ and the adsorption percentage (S, %) were calculated according to:

156 $$Q_e = \frac{V(C_0 - C_e)}{M} \tag{1}$$

157 $$S = \frac{C_0 - C_e}{C_0} \times 100 \tag{2}$$

158 Where: C_0 and C_e are the initial and equilibrium concentration of heavy metals (mg L^{-1}),

159 V is the volume of adsorption solution (mL), and M is the weight of biochar (g).

160 **3. Results and discussion**

161 **3.1. Characteristics of biochars**

162 The product yields of BC300, BC450 and BC600 were 67.6 %, 49.5 % and 34.4 %,

163 respectively. The loss in yield was increased with the increase of pyrolysis temperature.

164 The surface chemical elements of biochar before and after adsorption were determined

165 by X-ray photoelectron spectroscopy (XPS). From the XPS survey spectra, the main

166 elements of pristine biochar were carbon (64.29%), oxygen (24.3%), potassium (9.46%),

167 nitrogen (1.53%), phosphorus (0.42%) and biochar after adsorption were carbon

168 (77.72%), oxygen (17.29%), nitrogen (2%), phosphorus (0.42%), lead (2.2%), cadmium

169 (0.36%), potassium (not detected because of the extremely low content). As shown in

170 Fig. 1, the binding energy of carbon functional groups changed in some extent after

171 adsorption, indicating the important role of carbon functional groups in adsorption

172 mechanisms. In addition, four peaks were observed in the C 1s XPS spectra, including

173 C−C (284.8 eV), C−O (286.5 eV), C=O (288.4 eV), O−C=O (290.3eV). The XPS

174 survey spectra (Fig. 2) demonstrated that two new peaks appeared at the binding energy

175 of 139.7eV and 406.3eV after biochar sorption, which presented the existence of Pb4f

176 and Cd3d, respectively. Moreover, this adsorption process was favourable to the

177 removal of Pb because the peak area of Pb was higher than that of Cd.

178   Scanning electron microscopy (SEM) images revealed that the surface

179 morphologies of biochar before and after adsorption had some obvious changes. As

180 shown in the Fig. S1a, the surface of biochar before heavy metal adsorption was

181 extremely rough and the pore structure of pristine biochar was highly inhomogeneous.

182 However, Fig. S1b and Fig. 2 showed that a layer of materials was covered on the

183 surface of biochar, which may attribute to the adsorption of Pb and Cd onto biochar.

184 Moreover, some flaky particles were observed on the surface of biochar after adsorption,

185   and the possible explanation was that the precipitation of heavy metals was formed on

186   the surface of biochar. Therefore, multiple adsorption mechanisms should be

187   responsible for the Pb and Cd removal.

188   The BET characteristics of BC450 were presented in table S1. The BET surface

189   area of the BC450 was 51.15 $m^2 g^{-1}$ and pore volume was 0.06667 $cm^3 g^{-1}$, which were

190   higher than many other biochars reported in studies. The surface area and pore volume

191   of the biochar in the present study were larger than those of sugarcane bagasse.[10] The

192   pore volume of the biochar was greater than these of the biochars produced from wood

193   and bark of pine oak.[17]

194   The FTIR spectra of BC300, BC450 and BC600 were shown in Fig. 3. Different

195   wavenumbers were observed in the same functional groups of three biochars.

196   Characteristic peak of BC450 at 3417.3 cm^{-1} was due to the stretching vibration of −OH

197   groups. The band at 1618 cm^{-1} was related to the stretching vibration of −OH

198   deformation of water and C=O stretching vibration of the carbonyl from the carboxyl

199   group in biochars.[18] The peak at 1434.8 cm^{-1} was connected with COO− groups and the

200   broad band near at 1083.8 cm^{-1} may be attributed to the C−O bending vibration or the

201   band of the out-of-plane bending for carbonates (CO_3^{2-}) or to the P−O bond of

202   phosphate in biochars,[19,20] which was consistent with the high surface P contents of

203   BC450 indicated by the XPS results. Moreover, there was a new band at 875.5 cm^{-1}

204   when the pyrolysis temperature was above 450 ^{o}C, which was related to γ-CH furan.[21]

205   These heterocyclic compounds were a weak cation-π binder. Furthermore, the peak at

206   3417.3 cm^{-1} and 1618 cm^{-1} became weak because of the reduction of

207   oxygen-containing functional groups especially the disappearance of hydroxyl.

208   The FTIR spectra of BC450 before and after Cd, Pb and the mixture adsorption

209   were presented in Fig. 4. The band at 3417.3 cm^{-1} shifted to the higher wavenumbers

210   after adsorption. Those peaks, such as C=O, −OH, and COO−, shifted slightly to the

211   lower wavenumbers. After adsorption, a new peak at around 2360 cm^{-1} was found,

212   which could be assigned to C≡C in-line deformation vibration or carbon dioxide.[18]

213   These results indicated that the main adsorption mechanism was highly related to the

214   functional groups of biochar.

215   **3.2. Effect of pH on the adsorption of heavy metals**

216   The pH is a major factor affecting adsorption of heavy metals on aqueous solutions.

217   The adsorption capacity of Cd (II) and Pb (II) increased with the increase of system pH

218   **(**Fig. 5a**)**. The zero point of zeta potential (pH$_{zpc}$) was 2.3 for BC450 (Fig. 5b). When the

219   solution pH < pH$_{zpc}$, the biochar surface contained positive charge because of the

220   protonation of biochar's hydrated surface. Therefore, a strong electrostatic repulsion

221   occurred between positive charged biochar surface and cationic Pb (II) or Cd (II) ions,

222   which could be responsible for the lowest adsorption capacity at pH 2.0. Moreover,

223   abundant of H$^+$ in this solution could compete with Pb^{2+} and Cd^{2+} for available

224   adsorption sites on biochar. However, biochar became negative charge due to the

225   deprotonation of adsorbent's hydrated surface when pH > pH$_{zpc}$. The capacity of

226   electrostatic attraction increased with the increasing of pH value, indicating a positive

227   correlation between adsorbate and adsorbent. Considering the formation of precipitate

228   of high concentration Pb and Cd (e.g., 1 g L^{-1}) under a relative high pH value, pH 5.0

229   was chosen for Cd, Pb and the mixture of Pb and Cd.

230   **3.3 Kinetic studies**

231   The kinetic of heavy metals sorption on biochars was simulated using pseudo first

232   order kinetic model and pseudo second order kinetic model.[22] These equations can be

233   expressed as follows:

234    $q_t = q_e(1 - e^{-k_1 t})$ (3)

235    $q_t = \dfrac{k_2 q_e^2 t}{1 + k_2 q_e t}$ (4)

236   where k_1 (min^{-1}) and k_2 (g mg^{-1} min^{-1}) are the rate constant of the pseudo first order and

237   the pseudo second order, q_t and q_e are the adsorption amounts (mg g^{-1}) at time t and

238   equilibrium, respectively.

239   The correlation coefficient (R^2) of the pseudo-second-order model was higher than

240   that of the pseudo-first-order model (Table 1), indicating the experimental data fitted

241   better to pseudo-second-order model. As shown in Fig. 6, both Cd (II) and Pb (II)

242   adsorption were rapidly happened within the beginning 6 h, and adsorption capacities

243   were 41.05 mg g^{-1} and 43.2 mg g^{-1}, respectively. Furthermore, the values of q_e

244   calculated from pseudo-second-order model (R^2=0.94) were more fitted in the

245   experimental q_e value, indicating that the mechanism of theses adsorption process

246   depended on the rate limited chemisorption, such as complexation and precipitation.[23]

247   **3.4 Adsorption isotherms**

248   Langmuir and Freundlich adsorption models were used to fit the heavy metals

249   adsorption isotherm data.

250   The Langmuir model:

251    $$q_e = \frac{q_{max} K_L C_e}{1 + K_L C_e}$$ (5)

252   The Freundlich model:

253    $$q_e = K_F C_e^{1/n}$$ (6)

254   where C_e is the equilibrium concentration (mg L^{-1}), q_e (mg g^{-1}) is the amount of heavy

255   metals adsorbed at equilibrium, q_{max} (mg g^{-1}) is the maximum adsorption capacity of

256   the solute. The K_L (L mg^{-1}) and K_F ((mg g^{-1}) (mg L^{-1})$^{-n}$) are the adsorption coefficients

257   of Langmuir model and Freundlich model, respectively. The n is the Freundlich linearity

258   constant related to the surface site heterogeneity.

259   The relative parameters calculated from Langmuir model and Freundlich model

260   were listed in Table 2. It obviously demonstrated that all biochars' correlation

261   coefficient (R^2) values of Langmuir model at three temperatures were higher than those

262   of Freundlich model, which suggested that these adsorption data of heavy metals onto

263   biochars fitted Langmuir model better than Freundlich model.

264   The Cd^{2+} and Pb^{2+} adsorption isotherms on different biochars at three temperatures

265   demonstrated that the amount of heavy metals adsorbed onto biochars (BC300, BC450,

266   and BC600) increased with the increasing of reaction temperature (25, 30, and 40 ^{o}C).

267   Langmuir isotherm and freundlich isotherm for the adsorption of Cd and Pb on biochars

268   at 30 ^{o}C were presented in Fig. 7. Table S3 presented the comparison of the maximum

269   Cd (II) or Pb (II) adsorption capacity of various adsorbents in the previous study. As

270   seen, the prepared water hyacinth biochars maintained much higher Cd (II) and Pb (II)

271   removal performance than many other adsorbent materials reported in the literature.

272   **3.5 Effect of pyrolysis temperature on biochars' adsorption**

273   The physicochemical properties of biochar (porous structure, surface areas,

274   element contents, cation exchange capacity and pH) are dependent on the pyrolytic

275   temperature.[24,25] Ahmad, et al. demonstrated that biochar of higher pyrolytic

276   temperature had higher hydrophobicity, surface area, pore volume, pore size together

277   with low polarity that may have increased trichloroethylene adsorption from water.[26]

278   Kim, et al. reported that pH and surface area of biochar increased greatly at pyrolytic

279   temperature over 500 $^{\circ}$C, resulting in the increase of Cd adsorption capacity with

280   increasing pyrolytic temperature.[14]

281   In our study, BC450 showed the highest adsorption capacity, while BC300 had the

282   lowest adsorption amount. This phenomenon could be explained by the following

283   reasons: (1) the surface area of biochar increased and the porous structure of biochar

284   developed with the increase of pyrolysis temperature,[27] which may contribute to the

285   higher adsorption capacity; (2) there was a decrease of the amount of oxygen-containing

286   functional groups (carboxyl, hydroxyl and ether) when pyrolysis temperature was

287   increased. The disappearance of most oxygen-containing surface groups on BC600

288   would decrease heavy metals sorption onto biochar, though it had great surface area and

289   porous structure. However, the porosity and functional groups of BC300 were

290   incomplete, resulting in the lowest adsorption capacity comparing with BC450 and

291   BC600. Therefore, the main mechanism for heavy metals adsorption was not the pore

292   structure, but the reaction between heavy metals and surface functional groups.[28] These

293   data calculated from isotherms process demonstrated that biochar properties were

294   significantly influenced by pyrolysis temperatures, which played an important role in

295   affecting adsorption characteristics.

296   **3.6. Adsorption thermodynamic analysis**

297   The thermodynamic data, such as Gibbs free energy ΔG^0, enthalpy ΔH^0, entropy

298   ΔS^0, can be calculated using the following equations:

299    $\quad \Delta G^0 = -RT \ln K_e$ $\hspace{8cm}$ (7)

300    $\quad \ln K_e = \dfrac{\Delta S^0}{R} - \dfrac{\Delta H^0}{RT}$ $\hspace{6.5cm}$ (8)

301   Where ΔG^0 is the stand free energy change of the ion exchange (kJ mol^{-1}), ΔH^0

302   (kJ mol^{-1}) is the enthalpy change, ΔS^0 (J mol^{-1} K^{-1}) is the entropy change, R is the

303   universal gas constant (8.314 mol^{-1} K^{-1}), T is the absolute temperature (K), K_e is the

304   thermodynamic equilibrium constant which was calculated by plotting $\ln(q_e c_e^{-1})$ versus

305   q_e and extrapolating to zero q_e. The values of ΔH^0 and ΔS^0 can be determined from the

306   intercept and slope of the linear plot of ΔG^0 versus T.

307   Thermodynamic parameters were shown in Table S2. The negative values of ΔG^0 at

308   three different temperatures indicated that the process of these adsorption were

309   spontaneous in nature. Moreover, the values of ΔG^0 decreased with the increasing

310   reaction temperature (25, 30, and 40 $^{\circ}$C), which demonstrated that adsorption efficiency

311 was higher in high temperature than that of in low temperature. The endothermic

312 adsorption process was demonstrated by the positive value of ΔH^0 (Cd: 11.51 kJ mol^{-1};

313 Pb: 9.375 kJ mol^{-1}). Furthermore, the positive value of ΔS^0 presented the increasing

314 randomness at the solution/solid interface during the adsorption. From these

315 thermodynamic parameters, It can be concluded that these adsorption processes are

316 spontaneous and endothermic.

317 **3.7. Effect of background ionic strength on heavy metal removal**

318 As shown in Fig. S2, the NaCl had little influence on Cd^{2+} removal until the

319 concentration of NaCl was 0.5 mol L^{-1}, and the removal capacity was reduced from

320 43.40 mg g^{-1} to 34.30 or 19.54 mg g^{-1} while the concentration of NaCl was 0.5 mol L^{-1}

321 or 1 mol L^{-1}. However, the effect of NaCl on Pb^{2+} adsorption was more sensitive even

322 at a relative low NaCl concentration (0.05 mol L^{-1}). The adsorption capacity of Pb^{2+}

323 was 46.66 mg g^{-1} while no background ionic was dissolved, but the result dropped to

324 28.50 mg g^{-1} at 1 mol L^{-1} NaCl. The reason could be attributed to high concentrations

325 of Cl$^-$ and Na$^+$ which could hinder the electrostatic between the charges on biochar

326 surface and heavy metals ions in solution. In addition, Cl$^-$ and Na$^+$ could preempt

327 surface adsorption sites of adsorbent before heavy metals ions react with biochar.

328 Moreover, the high ionic strength of the solution could influence the activity coefficient

329 of Cd^{2+} and Pb^{2+}, thus decreasing the collide and contact between the sorbent and

330 solute;

331 **3.8. Desorption studies**

332   In order to analyze the desorption properties of water hyacinths biochar, desorption

333   studies were conducted in 0.5 mol L^{-1} hydrochloric acid. Desorption efficiency were

334   presented in Fig. S3, it showed that the maximum desorption capacity of Pb^{2+} was

335   92.01% (95.46 mg g^{-1}) for BC450. Furthermore, the lowest desorption efficiency of

336   Cd^{2+} was BC600, while that of Pb^{2+} was BC300, which could be assigned to the

337   biochar' physicochemical properties, such as the specific surface area, pore volume and

338   the functional group. Moreover, desorption efficiency of Pb^{2+} were higher than that of

339   Cd^{2+}. These results indicated that WH biochar had a potential of regeneration for Cd^{2+}

340   and Pb^{2+} adsorption.

341   **3.9. Possible mechanisms for competitive adsorption of Cd and Pb**

342   The mutual effects of coexisting Pb^{2+} and Cd^{2+} on adsorption of each other were

343   evaluated and the results were shown in Fig. 8a and b. In comparison with the single

344   system, the coexistence of Pb^{2+} and Cd^{2+} could influence the adsorption capacity each

345   other, which demonstrated the competitive adsorption between Pb^{2+} and Cd^{2+}. Moreover,

346   the effects of the coexistence of Pb^{2+} and Cd^{2+} at lower concentrations (0.25 mmol L^{-1})

347   decreased with the increase of adsorbents concentrations. While at higher

348   concentrations (0.5 mmol L^{-1}), this phenomenon was not obvious. Furthermore,

349   compared to the influence of Cd^{2+} on Pb^{2+} adsorption (Fig. 8b), the uptake of Cd^{2+} had a

350   greater influence after Pb^{2+} addition (Fig. 8a). The difference suggested that the

351   adsorption process in the mixture (Cd^{2+} and Pb^{2+}) was more favorable for Pb^{2+}. Therefore,

352   a complexation interaction would probably occur in binary system.

353   Multiple mechanisms are involved in heavy metal sorption onto biochar, e.g., ion

354   exchange, electrostatic attraction, surface complexation, physical adsorption,

355   co-precipitation, surface precipitation and innersphere complexation.[29-31] The schematic

356   illustration of Cd and Pb sorption mechanisms was shown in Fig. 9. In our study, the

357   FTIR spectra shown that the bands of oxygen-containing functional groups shifted

358   marginally before and after adsorption, indicating carboxyl (−COOH) and/or hydroxyl

359   (−OH) functional groups may be involved in coordination with Cd^{2+} and Pb^{2+} due to the

360   complexation.[32] Furthermore, Cao, et al. demonstrated that the coordination between the

361   oxygen-containing functional groups and heavy metals (e.g., Cd^{2+} and Pb^{2+}) was usually

362   accompanied with the release of H^+, resulting in the decrease of solution pH.[16] As

363   presented in Fig. S4, the solution pH of the blank system without heavy metals increased

364   after biochar addition, resulting from the mineral ash from pyrolysis. However, the

365   solution pH of the heavy metals sorption system decreased which compared to that of

366   blank system.[33] Therefore, complexation may be one of the main adsorption

367   mechanisms.

368   Moreover, before Pb and Cd adsorption, there is one peak in the O 1s spectrum at a

369   binding energy about 532.7 eV. After Pb and Cd adsorption, a peak is observed at a

370   binding energy greater than 532.4 eV. This indicated that some O atoms existed in a more

371   oxidized state because of Pb or Cd adsorption. As a result of the formation complexes in

372   reactions, in which a lone pair of electrons in the oxygen atom was donated to the shared

373   bond between O and Pb or Cd, and then the electron cloud density of the oxygen atom was

374   reduced, resulting in a lower binding energy peak observed.[34] Furthermore, the

375   compound combined with the shared bond between Pb and O is more stable than that of

376   formed between Cd and O, according to the linear relation of the cationic radii on the

377   coordination number, as well as the relation between bond length and bond strengths for

378   cation-oxygen bonds.[35] Therefore, these reasons may be mainly contributed to the

379   competitive adsorption which was favorable for Pb^{2+}.

380   Considering the amount of Cd^{2+} and Pb^{2+} adsorbed on biochar increased with the

381   increase of pH values (Fig. 5a), Electrostatic attractions may play a significant role in

382   sorption preferences. Furthermore, the amount of Pb^{2+} adsorbed on biochar was higher

383   than Cd^{2+} at pH 2.0−5.0. The higher Pb^{2+} adsorption may be related to the larger size of

384   the Pb^{2+} ion (Pb^{2+}: 1.32 Å; Cd^{2+}: 1.03 Å), which could induce the Pb^{2+} aquo-cation to

385   simultaneously interaction electrostatically with a larger number of neighboring

386   adsorption sites, thus stabilizing the adsorbed state.

387   The cyclic aromatic π-system could act as the π-donor to interact with heavy metal

388   ions, which could serve as the π-acceptor due to their electron deficiency. As shown in

389   Fig. 4, the weak band at 875.5 cm^{-1} was assigned to γ-CH of furan. The intensity of the

390   peak at 875.5 cm^{-1} became weak after Pb adsorption, likely related to the bands of C=C

391   stretching vibration in aromatic moieties,[32] while that of Cd loading became strong.

392   However, the band at 875.5 cm^{-1} became strong after the mixture of Cd^{2+} and Pb^{2+}

393   loading. According to the band changes in the heavy metal loading biochars, it can be

394   concluded that cation-π interaction might be responsible for Cd^{2+} and Pb^{2+} sorption. The

395 heterocyclic compound of γ-CH of furan was a weak cation-π binder, and may easily

396 bind with Cd^{2+} compared with Pb^{2+} (binding energy: $Cd^{2+} < Pb^{2+}$).[36] These results

397 showed that cation-π interaction was favorable for Cd^{2+}.

398 In addition, a new band at 684.6 cm^{-1} was observed after Pb^{2+} and the mixture

399 sorption, which may present new Pb precipitates. Precipitation would occur between

400 heavy metals and some ionized anions (e.g., CO_3^{2-} and PO_4^{3-}) released from the

401 minerals in biochars. Zhang, et al. reported that Cd precipitation as $CdCO_3$, $Cd_3(PO_4)_2$,

402 and probably $Cd(OH)_2$ could be responsible for Cd adsorption on water hyacinths

403 biochar produced at 450 $^{\circ}$C,[37] which were consistent with the existence of CO_3^{2-} and

404 P−O of phosphate analyzed by FTIR spectra. Moreover, Compared to $Pb(OH)_2$, the

405 precipitate formed between Cd^{2+} and OH^- was less soluble, according to the stability

406 constants (pK_{sp}) ($Cd(OH)_2$: 14.28; $Pb(OH)_2$: 14.93). Similarly, the stability of $CdCO_3$

407 (pK_{sp}: 12.00) and $Cd_3(PO_4)_2$ (pK_{sp}: 32.60) were higher than that of $PbCO_3$ (pK_{sp}: 13.13)

408 and $Pb_3(PO_4)_2$ (pK_{sp}: 42.10).[34] Therefore, it can be speculated that Cd^{2+} was prior to

409 forming theses precipitates, which could inhibit Pb^{2+} sorption.

410 As shown in Table 3, cation exchange may be responsible for the reaction

411 mechanisms of Cd^{2+} and Pb^{2+} removal. However, the contribution of cation exchange

412 occupied a relatively small percentage in the total metals adsorbed. Moreover, the net

413 amount of cations released from Pb^{2+} sorption onto biochar was higher than that of Cd^{2+}

414 sorption onto biochar, indicating cation exchange was favorable for Pb^{2+}. The possible

415 main reason may be that surface complexation between Cd or Pb and the oxygen groups

416   is most likely through Cd or Pb exchange with the complexed cations contained in

417   biochar (Fig. 9), and the complexing capacity of Pb is stronger than that of Cd.

418   Competitive adsorption may depend on such factors as ionic radius, ionic potential,

419   chemical properties and hydrolysis state. The lower Pb^{2+} ionic charge/radius ratio (3.3)

420   versus Cd^{2+} (1.9) leads to weaker Cd^{2+} ionic interaction forces versus Pb^{2+}, thus Pb^{2+}

421   would be retained on more surface sites with weaker negative charge. In this study, the

422   declined sorption capacity of Cd^{2+} in binary system were mainly attributed to the prior

423   interactions between Pb^{2+} and oxygen-containing functional groups, and stronger

424   complexing capacity of Pb^{2+}, as well as the prior electrostatic attractions between Pb^{2+}

425   and surface adsorption sites with negative charge. However, the competition from the

426   interactions of precipitate and cation-π should be responsible for the decrease of Pb^{2+}

427   adsorption capacity. Therefore, these reasons may be contributed to the results in binary

428   systems that the adsorption process was more favorable for Pb^{2+}.

429   **4. Conclusion**

430   This study proved that BC450 had the highest adsorption capacity for heavy metal

431   compared to BC300 and BC600. Both in single and in binary system, Pb^{2+} had a higher

432   amount of adsorption on WH biochar compared with Cd^{2+}, and the coexistence of Pb^{2+}

433   and Cd^{2+} could affect adsorption capacity of each other. Furthermore, the existence of

434   Pb^{2+} inhibited the sorption of Cd^{2+}, which could be attributed to the complexation,

435   cation exchange, and electrostatic attraction. However, the sorption of Pb^{2+} was affected

436   by the existence of Cd^{2+}, which may result from the precipitate and cation-π interaction.

437　**Acknowledgements**

438　　This study was financially supported by the National Natural Science Foundation

439　and innovative group of china (Grant no.41271332, 51478470 and 51521006) and the

440　Hunan Provincial Innovation Foundation For Postgraduate (Grant No. CX2015B090

441　and CX2015B095).

442　**Reference**

443　1.　L. Wang, J. Zhang, R. Zhao, Y. Li, C. Li and C. Zhang, *Bioresour. Technol.*, 2010,

444　　　101, 5808–5814.

445　2．D. Mohan, H. Kumar, A. Sarswat, M. Alexandre-Franco and C. U. Pittman, *Chem.*

446　　　*Eng. J.*, 2014, 236, 513–528.

447　3.　W. Zhang, S. Mao, H. Chen, L. Huang and R. Qiu, *Bioresour. Technol.*, 2013, 147,

448　　　545–552.

449　4.　R. C. Brändli, G. D. Breedveld and G. Cornelissen, *Environ. Toxicol. Chem.*, 2009,

450　　　28, 503–508.

451　5.　M. Kobya, E. Demirbas, E. Senturk and M. Ince, *Bioresour. Technol.*, 2005, 96,

452　　　1518–1521.

453　6.　X. Cao, L. Ma, B. Gao and W. Harris, *Environ. Sci. Technol.*, 2009, 43, 3285–3291.

454　7.　H. Wang, K. Lin, Z. Hou, B. Richardson and J. Gan, *J. Soil. Sediment.*, 2010, 10,

455　　　283–289.

456　8.　M. Ahmad, S. S. Lee, X. Dou, D. Mohan, J. K. Sung, J. E. Yang and Y. S. Ok,

457　　　*Bioresour. Technol.*, 2012, 118, 536–544.

458   9.   M. H. Duku, S. Gu and E. B. Hagan, *Sust. Energy Rev.*, 2011, 15, 3539–3551.

459   10. Y. Xue, B. Gao, Y. Yao, M. Inyang, M. Zhang, A. R. Zimmerman and K. S. Ro,

460   *Chem. Eng. J.*, 2012, 200, 673–680.

461   11. X. Dong, L. Q. Ma and Y. Li, *J. Hazard. Mater.*, 2011, 190, 909–915.

462   12. C. Gan, Y. Liu, X. Tan, S. Wang, G. Zeng, B. Zheng, T. Li, Z. Jiang and W. Liu, *RSC*

463   *Advances.*, 2015, 5, 35107–35115.

464   13. X. Chen, G. Chen, L. Chen, Y. Chen, J. Lehmann, M. B. McBride and A. G. Hay,

465   *Bioresour. Technol.*, 2011, 102, 8877–8884.

466   14. W. K. Kim, T. Shim, Y. S. Kim, S. Hyun, C. Ryu, Y. K. Park and J. Jung, *Bioresour.*

467   *Technol.*, 2013, 138, 266–270.

468   15. G. Yang, L. Tang, G. Zeng, Y. Cai, J. Tang, Y. Pang, Y. Zhou, Y. Liu, J. Wang, S.

469   Zhang, *Chem. Eng. J.*, 2015, 259, 854–864.

470   16. X. Cao, L. Ma, B. Gao and W. Harris, *Environ. Sci. Technol.*, 2009, 43, 3285–3291.

471   17. D. Mohan, C. U. Pittman, M. Bricka, F. Smith, B. Yancey, J. Mohammad, P. H.

472   Steele, M. F. Alexandre-Franco, V. Gomez-Serrano and H. Gong, *J. Colloid*

473   *Interface Sci.*, 2007, 310, 57–73.

474   18. L. Tang, G. D. Yang, G. M. Zeng, Y. Cai, S. S. Li, Y. Y. Zhou, Y. Pang, Y. Y. Liu, Y.

475   Zhang and B. Luna, *Chem. Eng. J.*, 2014, 239, 114–122.

476   19. T. Y. Jiang, J. Jiang, R. K. Xu and Z. Li, *Chemosphere*, 2012, 89, 249–256.

477   20. B. Wen, J. Zhang, S. Zhang, X. Shan, S. U. Khan and B. Xing, *Environ. Sci.*

478   *Technol.*, 2007, 41, 3165–3171.

479   21. M. Uchimiya, I. M. Lima, K. K. Thomas, S. Chang, L. H. Wartelle and J. E.

480   Rodgers, *J. Agric. Food Chem.*, 2010, 58, 5538–5544.

481   22. Y. S. Ho and G. McKay, *Process. Biochem*, 1999, 34, 451–465.

482   23. D. Kołodyńska, R. Wnętrzak, J. Leahy, M. Hayes, W. Kwapiński and Z. Hubicki,

483   *Chem. Eng. J.*, 2012, 197, 295–305.

484   24. K. H. Kim, J. Y. Kim, T. S. Cho and J. W. Choi, *Bioresour. Technol.*, 2012, 118,

485   158–162.

486   25. H. Yuan, T. Lu, D. Zhao, H. Huang, K. Noriyuki and Y. Chen, *J. Mater. Cycles

487   Waste.*, 2013, 15, 357–361.

488   26. M. Ahmad, S. S. Lee, A. U. Rajapaksha, M. Vithanage, M. Zhang, J. S. Cho, S. E.

489   Lee and Y. S. Ok, *Bioresour. Technol.*, 2013, 143, 615–622.

490   27. P. Bonelli, E. Buonomo and A. Cukierman, *Energy Sour.*, 2007, *Part A* 29, 731–740.

491   28. D. Sud, G. Mahajan and M. Kaur, *Bioresour. Technol.*, 2008, 99, 6017–6027.

492   29. H. Lu, W. Zhang, Y. Yang, X. Huang, S. Wang and R. Qiu, *Water Res.*, 2012, 46,

493   854–862.

494   30. X. Tan, Y. Liu, G. Zeng, X. Wang, X. Hu, Y. Gu and Z. Yang, *Chemosphere*, 2015,

495   125, 70–85.

496   31. H. Zheng, Z. Wang, X. Deng, J. Zhao, Y. Luo, J. Novak, S. Herbert and B. Xing,

497   *Bioresour. Technol.*, 2013c, 130, 463–471.

498   32. Z. Wang, G. Liu, H. Zheng, F. Li, H. H. Ngo, W. Guo, C. Liu, L. Chen and B. Xing,

499   *Bioresour. Technol.*, 2015, 177, 308–317.

500   33. J. H. Yuan, R. K. Xu, H. Zhang, *Bioresour. Technol.*, 2011, 102, 3488–3497.

501   34. L. Jin and R. Bai, *Langmuir.*, 2002, 18, 9765–9770.

502   35. J. Zio, *J. Solid State. Chem.*, 1985, 57, 269–290.

503   36. J. C. Ma and D. A. Dougherty, Chem. Rev., 1997, 97, 1303–1324.

504   37. F. Zhang, X. Wang, D. Yin, B. Peng, C. Tan, Y. Liu, X. Tan and S. Wu, *J. Environ.*

505   *Manage.*, 2015, 153, 68–73.
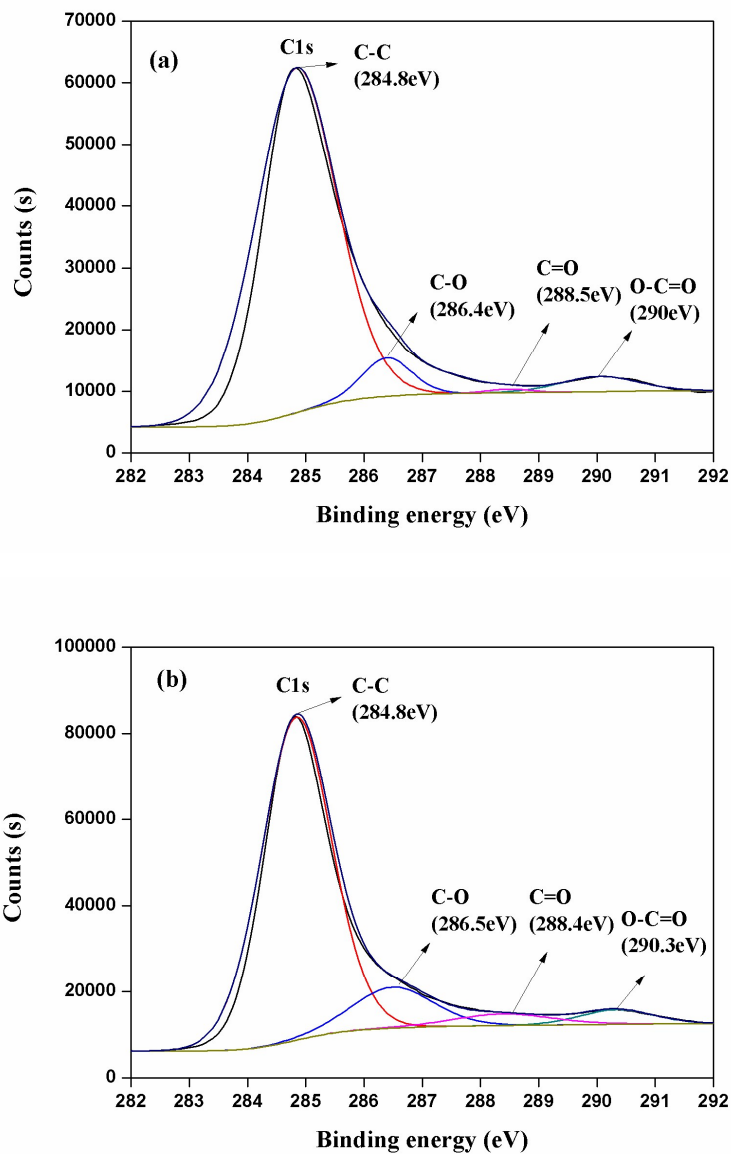
Fig. 1. C 1s XPS spectra of BC450 (a) before and (b) after adsorption.
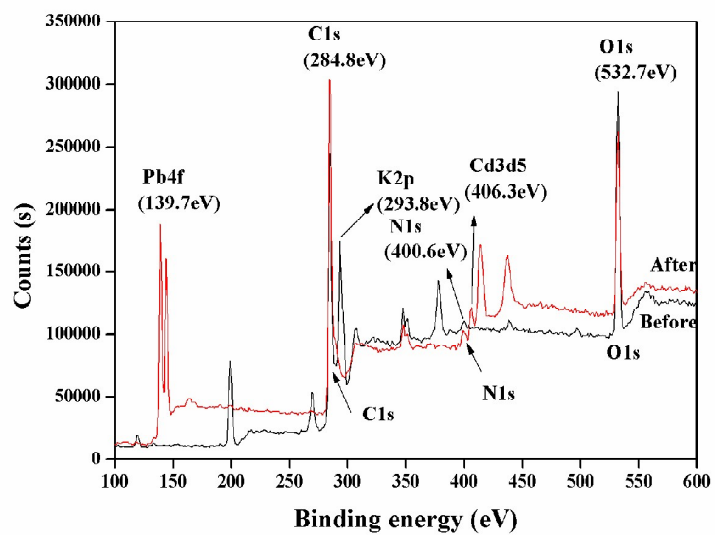
Fig. 2. XPS survey spectra of BC450 before and after adsorption.
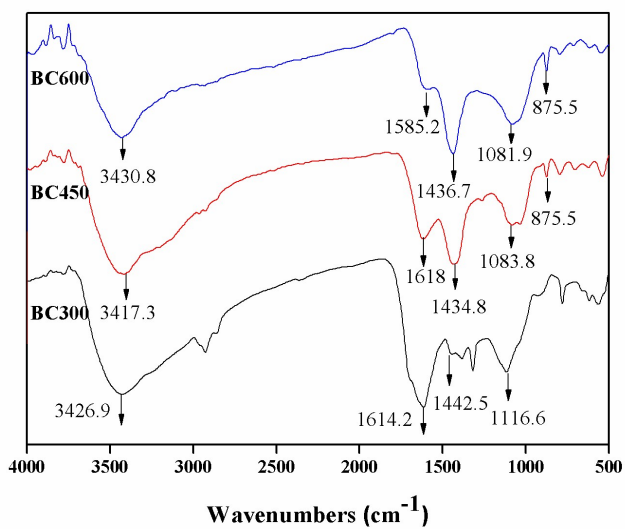
Fig. 3. FTIR spectra of BC300, BC450 and BC600.
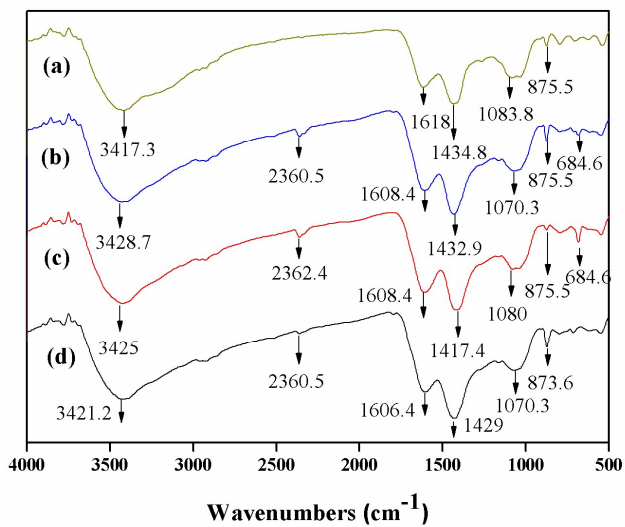
Fig. 4. FTIR spectra of BC450 (a) before and after (b) the mixture, (c) Pb and (d) Cd adsorption.
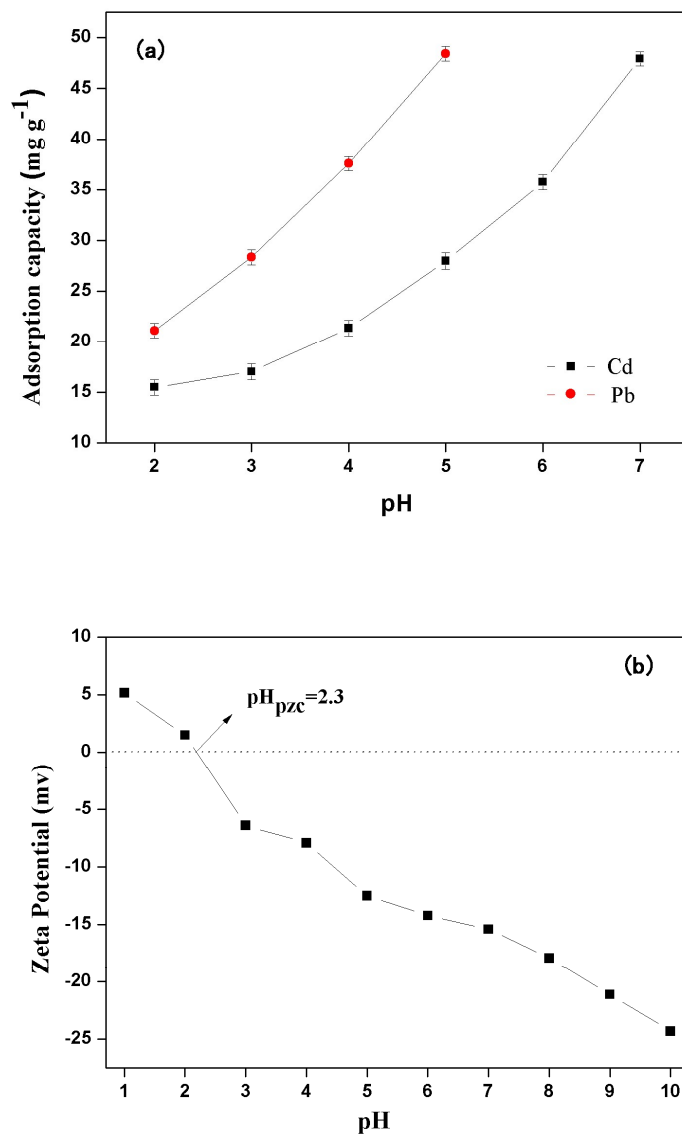
Fig. 5. (a) Effect of initial solution pH values on Cd and Pb adsorption by BC450. (b) Zeta potentials

of BC450 at different solution pH values.
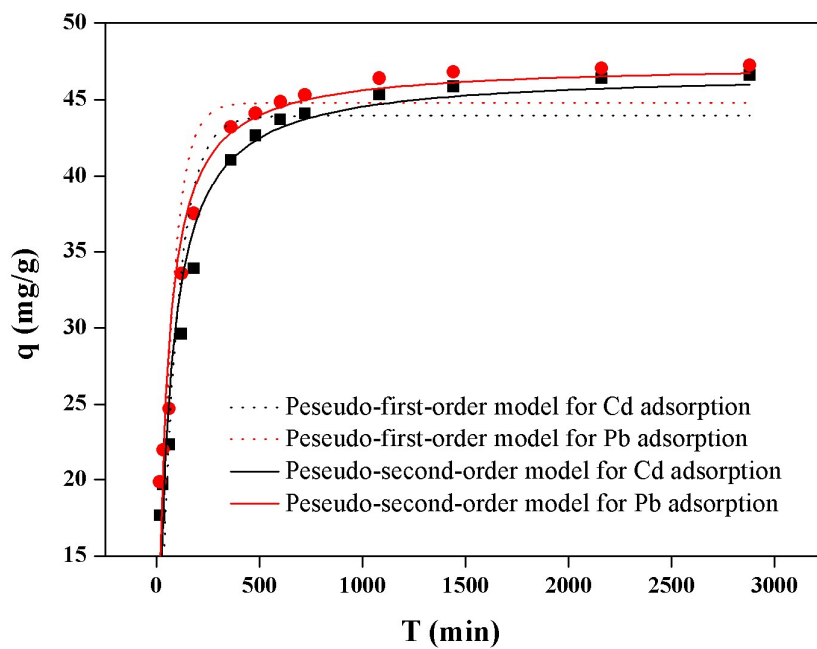
Fig. 6. Pseudo-first-order sorption kinetics and pseudo-second-order sorption kinetics for Cd and Pb adsorption onto BC450 in single system (initial heavy metals concentration: 100 mg L^{-1}; pH: 5.0; reaction temperature: 30 ^{o}C).

.
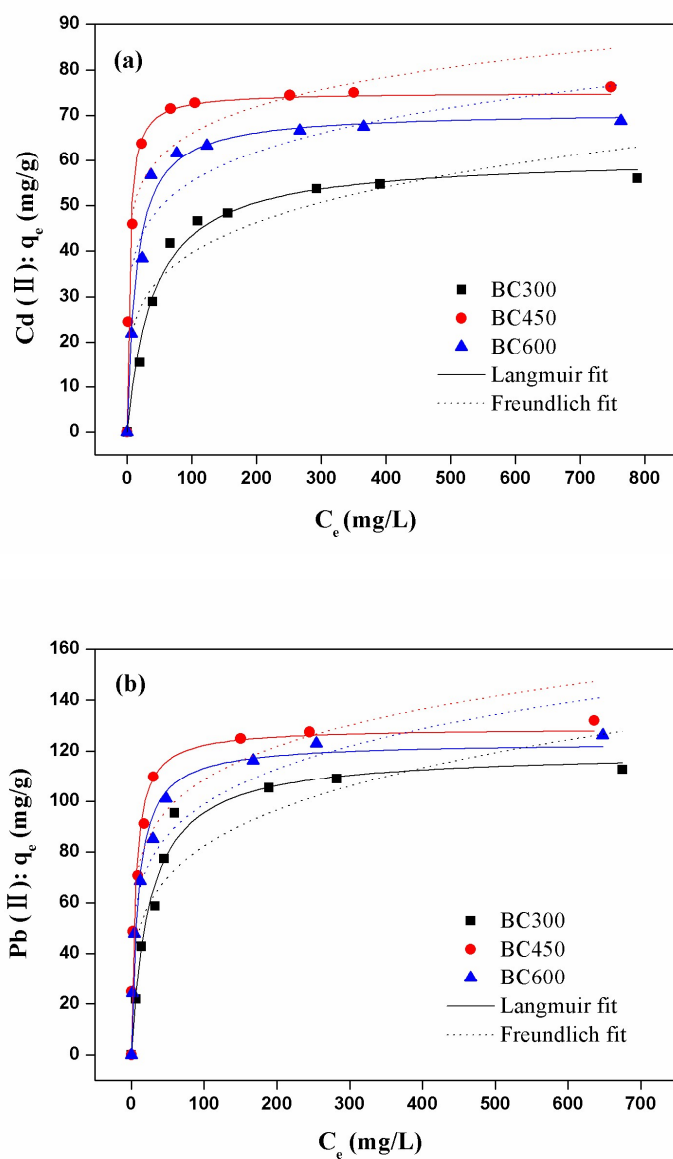
Fig. 7. Langmuir isotherm and freundlich isotherm for the adsorption of Cd and Pb on biochars at 30 ^{o}C (solution volume: 50 mL; adsorbent dose: 0.1 g; contact time: 24 h; pH: 5.0).
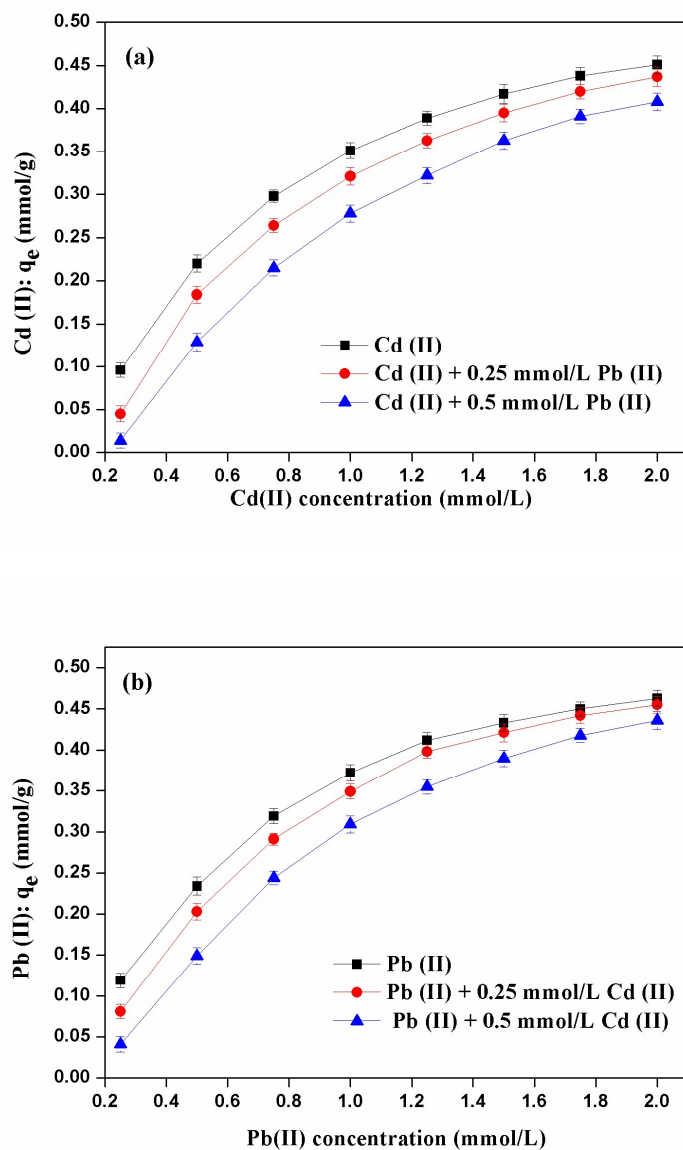
Fig. 8. (a) Effect of Pb (II) on Cd (II) adsorption by BC450 (solution volume: 50 mL; adsorbent dose: 0.1 g; contact time: 24 h; pH: 5.0; rpm: 140). (b) Effect of Cd (II) on Pb (II) adsorption by BC450 (solution volume: 50 mL; adsorbent dose: 0.1 g; contact time: 24 h; pH: 5.0; rpm: 140).
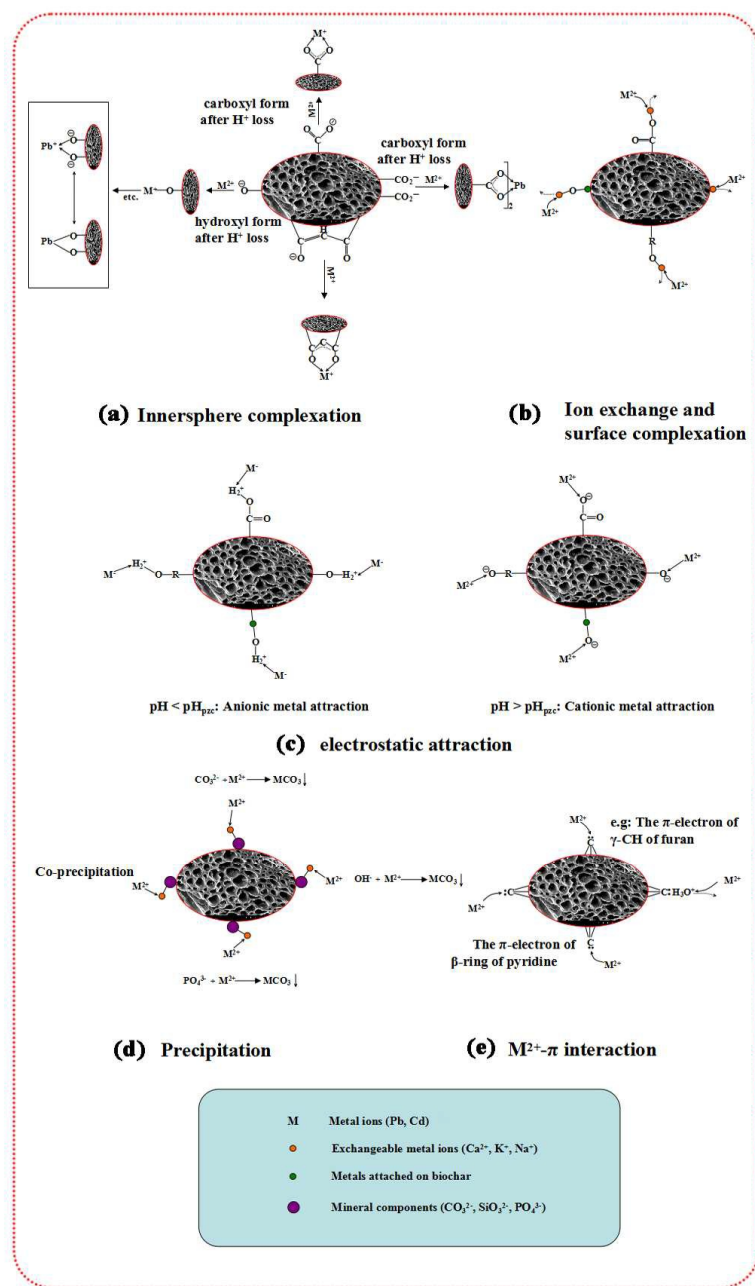
Fig. 9. The schematic illustration of Cd and Pb sorption mechanisms.

Table 1 Pseudo-first-order and pseudo-second-order model parameters for Cd (II)

and Pb (II) adsorption on BC450 at 30 $^{\circ}$C.

Pollutants	Pseudo-first-order			Pseudo-second-order		
	K_1 (min^{-1})	q_e (mg g^{-1})	R^2	K_2 (g mg^{-1} min^{-1})	q_e (mg g^{-1})	R^2
Cd(II)	0.01235	43.94	0.84	0.0004233	46.79	0.94
Pb(II)	0.01629	44.78	0.82	0.0005578	47.33	0.94

Table 2 Langmuir and Freundlich isotherms parameters for Cd^{2+} and Pb^{2+} sorption

on WH biochars (BC300, BC450, BC600) at 30 ^{o}C.

Pollutants	Biochars	Langmuir model			Freundlich model		
		Q_{max} (mg g^{-1})	K_L (L mg^{-1})	R^2	K_F (L mg^{-1})	n	R^2
Cd	BC300	60.85	0.0249	0.98	14.09	4.453	0.75
	BC450	74.99	0.2786	0.98	37.38	8.093	0.78
	BC600	70.77	0.0712	0.98	26.47	6.239	0.71
Pb	BC300	119.58	0.0397	0.98	28.49	4.340	0.78
	BC450	128.95	0.1815	0.97	50.86	6.069	0.87
	BC600	123.37	0.1110	0.98	41.09	5.245	0.87

Table 3 Net cations release from Cd or Pb sorption onto biochar BC450

Heavy metals	The net amount of metal cations released (mmol g^{-1})					Total heavy metals adsorbed (mmol g^{-1})
	$2K^+$	Ca^{2+}	$2Na^+$	Mg^{2+}	Total	
Pb	0.576	0.108	0.087	0.062	0.833	6.684
Cd	0.489	0.113	0.081	0.056	0.739	5.379

Graphical Abstract